CRS Methodology to the Realmonte Salt mine, southwestern Sicily: an application for hydrogen storage potential site in Italy.

Authors: Anzelmo G.[1] , Cella G.M.[2], Magistroni C.[2], Da Pra A.[2] & Iacopini D[1].

Affiliations: [1] Dept. of Earth, Environmental and Resources Sciences of the University of Naples Federico II (Italy)
[2] ENI S.p.A, San Donato Milanese (Italy)

Keywords: CRS, Salt Caverns, H_2 Storage, Salt Mine.

*Corresponding author. E-mail address: giuseppa.anzelmo@unina.it

---

Peer-review status: *This manuscript is a preprint currently under review for publication in the International Journal of Hydrogen Energy. This version has not completed peer review and has not been formally accepted for publication; its content may differ from subsequent versions. If accepted, the final peer-reviewed version will be available via a DOI link on this page.*

CRS Methodology to the Realmonte Salt mine, southwestern Sicily: an application for hydrogen storage potential site in Italy.

Authors: Anzelmo G.[1] , Cella G.M.[2], Magistroni C.[2], Da Pra A.[2] & Iacopini D[1].

Affiliations: [1] Dept. of Earth, Environmental and Resources Sciences of the University of Naples Federico II (Italy)

[2] ENI S.p.A, San Donato Milanese (Italy)

Keywords: CRS, Salt Caverns, H_2 Storage, Salt Mine

Abstract:

As Sicily expands its renewable energy portfolio, the need for large-scale energy storage becomes increasingly urgent to ensure supply-demand balance. Hydrogen storage in salt caverns represents a promising solution in this context. This study presents the first real-world application of the Common Risk Segment (CRS) methodology, originally developed for oil and gas exploration and recently adapted for CO_2 storage site screening, to underground hydrogen storage in salt caverns, applied to the Realmonte salt mine in southwestern Sicily, Italy. The site's evaporitic sequence was subdivided into two stratigraphic units: the lower "First Cycle" (below -250 m b.s.l.) and the upper "Second Cycle" (above -250 m, encompassing the active mine). For each unit, a site card integrating 20 geological, rock salt, and environmental parameters was compiled, with impact values (-3 to +3), calibrated weights (1-3), and a six-class robustness scale (-2 to +3) quantifying data reliability. Normalised CRS scores were calculated as 95.81% for the First Cycle and 86.91% for the Second Cycle, confirming the deeper salt section as the only viable target for hydrogen storage. The Second Cycle is excluded because of insufficient top-salt depth and caprock thickness, as well as its operational incompatibility with the active mine. A Monte Carlo sensitivity analysis (500 runs per site) demonstrated the stability of the scoring system under data uncertainty, with coefficients of variation below 0.3% for all configurations tested. Cross-site benchmarking against two internationally operational hydrogen storage facilities, Teesside, UK (84.82%) and Clemens Dome, USA (91.62%), validated the methodology and confirmed that the inter-site ranking is preserved in 100% of simulation runs. The high score of the Realmonte First Cycle relative to these operational benchmarks reflects its thick, pure halite (>300 m) at optimal depth (400-600 m), absence of faulting, and strong caprock integrity.

A preliminary storage capacity estimate, based on cavern dimensions of 100-200 m height and 60-80 m diameter with a minimum spacing of three times the cavern diameter, yields a prospective capacity of 1.5-2.5 TWh for the First Cycle, sufficient to meet Sicily's projected hydrogen storage requirements through 2030 and strategically positioned near planned offshore renewable energy hubs. The results identify the Realmonte First Cycle as a priority candidate for pilot cavern development in the Italian hydrogen storage roadmap.

1. Introduction:

Hydrogen storage in salt caverns is currently considered one of the most technically and economically viable solutions for addressing the seasonal variability of renewable energy production, while also supporting frequent cycling over short- to medium-term timescales [1]. The main limitation of this solution lies in the uneven spatial distribution of suitable underground evaporitic formations. In Europe, a geospatial inventory of potential salt deposits has been developed based on geological and environmental criteria [2]. n Italy, however, preliminary screening of suitable sites is still at a very early stage.In this context, the application of the Common Risk Segment (CRS) approach at site scale provides a valuable tool for identifying the most favourable sub-areas and quantitatively assessing storage-related risks. This study represents the first application of the CRS methodology to a real-world case study of hydrogen storage in salt caverns, marking a significant step forward in the use of this tool beyond its previous applications to CO_2 storage. The Realmonte rock salt mine, located in southern Sicily, was selected as a test site because of its favourable geological and geomechanical characteristics and its proximity to the coastline, which is advantageous for brine management and technical operations during solution mining. From a conceptual perspective, the site shows promising characteristics for the development of hydrogen storage infrastructure.

Several recent studies have proposed frameworks for evaluating potential hydrogen storage sites in salt formations, yet significant methodological gaps remain. Caglayan et al. [3] estimated the technical potential of salt caverns for hydrogen storage across Europe using a GIS-based volumetric approach; however, their analysis relied on basin-scale geological parameters without site-specific risk scoring or geological model integration. Zhu et al. [4] developed an Entropy-Weighted TOPSIS model for site selection of salt cavern hydrogen storage in China, incorporating 15 evaluation indices, but their method is purely statistical and does not produce spatially resolved risk maps. Similarly, Huang et al. [5] proposed a "four-factor" AHP-based site selection system for salt cavern hydrogen storage at Pingdingshan, China, relying on expert-weighted indices rather than geological model outputs. Derakhshani et al. [6] applied machine-learning algorithms to assess salt cavern suitability for hydrogen storage in Poland, using eight classifiers on spatial datasets; while innovative, this approach requires large training datasets and does not incorporate subsurface geological models. Lankof et al. [7] assessed hydrogen storage potential in Polish salt domes through volumetric capacity estimation, addressing cavern convergence but not multi-parameter risk integration. Baek et al. [8], within the U.S. DOE SHASTA programme, proposed a qualitative Site Quality Assessment for salt cavern hydrogen storage, providing a checklist-based screening tool without quantitative scoring or spatial analysis.

A common limitation across these approaches is the lack of an integrated workflow linking a three-dimensional geological model to spatially resolved impact and risk maps through a quantitative multi-parameter scoring system. None of these methods produces a final composite risk map that can guide cavern placement at the site scale. The Common Risk Segment (CRS) methodology, originally developed for hydrocarbon play-based exploration [9], and recently adapted for CO_2 storage site screening [10] and recently applied to salt cavern hydrogen storage assessment [11,12], offers precisely this integration. While several studies have addressed salt cavern engineering aspects such as geomechanical design criteria [13,14], operational experience from existing facilities [15], and storage capacity modelling [16], none has applied a CRS-based integrated risk-mapping workflow to hydrogen storage in salt caverns.

By adapting the CRS workflow to salt cavern hydrogen storage, this study fills a gap in the current literature: it is the first application of CRS-based risk mapping specifically designed for evaluating hydrogen storage potential in evaporitic geological settings. The methodology presented here is intentionally general with respect to the stored gas: the site card parameters address the geological, rock salt, and environmental characteristics that govern the suitability of a salt cavern for any gas storage application (H_2, CAES, natural gas, CO_2). We did not include gas-specific geochemical parameters (e.g., hydrogen-rock salt reactivity, microbial consumption rates) precisely to maintain this transferability. Since hydrogen is the most demanding stored gas in terms of purity requirements and cycling frequency, a site that scores well for H_2 storage will also be suitable for less stringent applications.

This paper is Part 2 of a two-part study. Part 1 [34] presents the full methodological framework of the CRS approach adapted for salt cavern gas storage, including the derivation of the key-factor table, the definition of weight and impact scales, the construction of the site card, and the GIS-based risk calculation workflow. Part 1 also validates the sensitivity of the method through Monte Carlo simulation on two international benchmark sites (Teesside, UK and Clemens Dome, USA). The present paper (Part 2) applies this methodology to the Realmonte salt mine in Sicily, Italy, providing a complete site-specific assessment. While Part 2 is designed to be self-standing, readers are referred to Part 1 for the detailed derivation of the scoring system and the full sensitivity analysis framework.

This work aims to quantitatively assess the storage potential of the site through the integrated evaluation of all relevant geological, structural, and environmental parameters using the site card approach, combined with a spatial risk assessment to identify the most suitable zones, i.e., those associated with the lowest overall risk. For application purposes, the salt sequence was divided into two main stratigraphic units, an upper and a lower section, on the basis of thickness, in situ salt quality, and the presence of the currently active mine, which itself constitutes a major environmental and operational constraint. The CRS approach was then applied separately to assess the risks associated with cavern development in the shallower portion of the site (the "Second Cycle") and in the deeper halite-rich interval (the "First Cycle"). The following sections present the geological framework of the study area, describe the CRS-based methodology and results as individual and integrated risk maps, and finally compare the outcomes for the two stratigraphic units in the discussion.

1.1 The Sicilian energy scenario

Sicily provides a prominent example of energy storage efficiency, owing to its abundant Renewable Energy Sources (RES) in Italy [17]. By November 2024, Sicily led Italy in solar and wind RES, with 2,637 MW of photovoltaic and 2,462 MW of wind capacity. Photovoltaic and wind energy constitute 96% of new RES installations in 2024, representing 97% of the renewable capacity [1,17]. In recent years, regional policies have increasingly favoured the approval of renewable energy projects, both onshore and offshore, particularly wind farms [1]. From April to September, the productivity of these systems consistently exceeds local energy demand because of the island's favourable geographic setting [18]. This creates a strong incentive to develop hydrogen (H_2) energy storage as a means of managing renewable curtailment. Several onshore wind farms are already operational across northern and western Sicily, where average elevations are highest [17].
Further expansions and upgrades are planned in the northwestern provinces and in central Sicily, particularly in the Caltanissetta area. In addition, several offshore wind farm projects have been approved along the western and southern coasts facing the Strait of Sicily, an area known for strong winds and marine currents [17]. These include Eureka Wind [19], Bluwind Pozzallo [20], Ostro [21], 7Seas Med [22], Sicilia A [23], Sicily South [24], and Calypso [25], with approved turbine capacities ranging from 250 MW to 1200 MW. The most distant wind farm will be constructed 35 km offshore south of the Egadi Islands [18]. These initiatives provide a major opportunity for Sicily to establish itself as a renewable energy hub, contributing to the decarbonisation of the energy system while also supporting economic growth and job creation.
Another pathway currently under development is H_2 production by electrolysis, with plant capacities ranging from 1 MW to 100 MW, as in the Hynego and NextHy projects [26]. Hydrogen is a strategic component of the decarbonisation of industry and transport, but costs remain high. In Italy, the main challenges at both national and local scales include complex authorisation procedures and the absence of large, sustainable storage facilities, which could otherwise support the development of smart grids on the island and, more broadly, in southern Italy [27]. Regarding energy storage potential, although Sicily ranks sixth in Italy for battery use in energy storage, contributing 6.8% of the total 4,745 MW in Italy, its greatest potential lies in its geological structure. The island is the only emergent area in the Mediterranean, with the largest areal extension of Messinian salt deposits [28,29], which have

been exploited for alkaline salt extraction in large mines strategically distributed in its central-western and southern areas. These are the same areas where renewable energy production projects using wind power are being developed.

The current energy scenario in Sicily therefore requires new storage solutions to improve the efficiency of seasonal renewable production systems. In this context, storage in salt caverns appears to be one of the most practical options. This has directed attention to Sicily, which offers considerable geological promise because of its established salt deposits. Historically, these deposits have been studied mainly for scientific purposes rather than for storage applications. Against this background, the Realmonte area, located on the southern coast, was identified as a site of particular interest. The aim of this study is to apply the CRS methodology to determine whether, beyond the existing rock salt mine and at the broader site scale, the area has potential for future development of salt caverns for green hydrogen storage

2. Geological setting

The selected site is located along the southern coast of Sicily, between the towns of Realmonte and Siculiana, within the province of Agrigento, Italy. The area includes the Realmonte alkaline salt mine, one of the three remaining traditional underground mines with active chambers and galleries still operating on the island. Geologically, the site belongs to the Caltanissetta Basin, a NE-SW-trending structural depression filled mainly by evaporitic deposits related to the Messinian salinity crisis. This major geological event, caused by the temporary isolation of the Mediterranean Sea following closure of the Strait of Gibraltar between 5.97 and 5.33 Ma, led to the precipitation of thick interbedded salt layers [28,30]. Subsequent sedimentation included younger Plio-Pleistocene sands, clays, and carbonates.

As shown in the stratigraphic column of Fig. 1b, the Messinian evaporitic sequence at the Realmonte mine comprises a 400-600 m thick halite succession [31] that begins with pre-salt deposits (Tortonian and Miocene), predominantly of carbonate and clastic composition, followed by a 150-250 m thick unit of pure halite (NaCl). This is overlain by an 80-120 m thick interval in which halite is interlayered with finely laminated, strongly deformed K-Mg salt minerals, mainly kainite ($MgSO_4 \cdot KCl \cdot 3H_2O$), together with intercalated clayey layers. Upward, the succession is completed by a third halite unit, approximately 100 m thick, composed of nearly pure halite and corresponding to the orange lithologies shown in the geological sections of Fig. 1b. The salt units are capped by an overburden up to 180 m in thickness, consisting of gypsum, chalk, and clay, and overlaid by Trubi marls and Pleistocene mixed sands (depicted in green lime in Fig. 1b) [3,31,32,33]. Structurally, the salt body is deformed by a series of folds trending NW-SE, the largest of which is the Montallegro anticline, imparting a characteristic lens-shaped geometry to the deposit [34,35]. Figure 1b illustrates the stratigraphic architecture of the Realmonte salt succession through three geological sections, each oriented differently and encompassing the entire mining area. The cumulative thickness of the rock salt, spanning the "first" and "second" cycles, significantly exceeds 500 meters (with lithologies depicted in orange and light blue in the sections), and the apex of the deposit appears to deepen towards the coast. Presently, only the upper portion of the rock salt from the second cycle's halite is being extracted (as shown in Figure 1b, the east and west galleries of the mine that intersect the succession are depicted in 3D sections), whereas the entire lower portion remains unexploited. As shown in Fig 1a and b for a better characterization of the main key factor, a re-analysis of 40 well and sampling of rock units from the second cycle has allowed a better characterization of local stratigraphy and main structure in the area around the main active mine galleries. For the geological detailed structure, we do refer to the paper by Lugli et al [30].

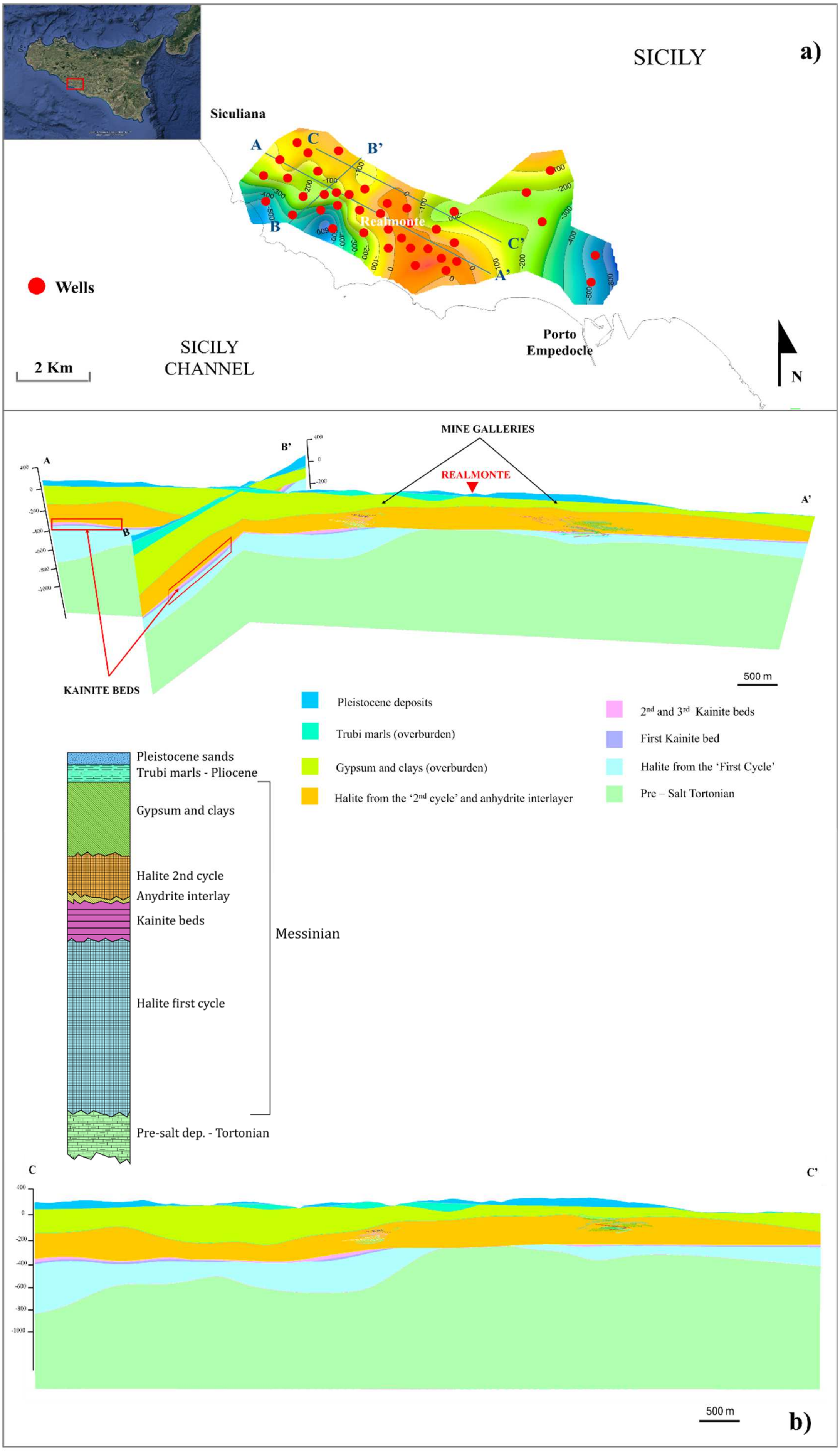

Fig, 1. a) Location of the Realmonte area and dataset consisting only of deep boreholes (in red dots). The map shows the distribution at the top of the salt layer with extremely shallow values. b) Geological sections A-A', B-B,' and C-C' show the stratigraphic architecture of the Realmonte succession reconstructed by interpolating borehole stratigraphies.

3. Methodology

The initial and essential step in our methodology, which is essential for both the compilation of tables and execution of calculations and algorithms for comprehensive risk assessment, involves the development of a geological model of the study area. In this instance, the dataset (fig. 1a) exclusively comprises stratigraphic data, derived from 40 deep boreholes drilled in the early 1970s, prior to the commencement of mining operations, and lacks geophysical logs. Point-by-point interpolation of the well data across the limited mine area allowed the generation of 2D surfaces, thickness maps, and facies maps, and, most importantly, a 3D geological model with a 20 m grid. Geological sections extracted from the model are shown in Fig. 1b. Analysis of the model revealed a clear distinction within the rock salt sequence, which can be divided into two sections: an upper segment and a lower segment. These segments, referred to as the second-cycle halite and first-cycle halite, respectively, exhibit distinct petrological and petrophysical characteristics, as inferred from the stratigraphic interpretations of the boreholes. The upper section is characterized by greater mineralogical heterogeneity, the presence of insoluble layers and kainite, and larger crystal sizes, whereas the lower section is purer and exhibits a microcrystalline salt fabric [30]. The top of the second-cycle halite was generally located at depths of less than 200 m, while the top of the deeper halite level was found at an average depth of approximately 350 m.

Environmental parameters impose constraints on the application of the block method to the entire sequence; consequently, in this study, the workflow is applied separately to the two salt levels, with the geological model accounting for significant variability. From the geological model, maps for each requisite geological, environmental, and salt-specific parameter were derived primarily and directly for subsequent phases of CRS application. These include the lithological map illustrating the 2D distribution of lithological variations at the roof depth of each halite level, thickness maps, maps of the salt top, and structural complexity maps, among others [34]. The environmental parameters and their respective maps were evaluated and reconstructed following a geographical and environmental study of the site, which encompassed the identification of any production wells in the area, protected zones, water availability (necessary for the solution mining phase of the caverns), and an assessment of the environmental and technical impact of the operating mine compared to a hypothetical hydrogen storage project in the area or within the same mining concession, but at depth.

Following this geological phase, the application of the Common Risk Segment method at Realmonte follows the workflow described by Anzelmo et al. [34], which is structured into three main stages:

(a) compilation of the key-factor table;

(b) formulation of a site card by assigning impact values to each geological, rock salt, and environmental parameter identified in the previous step, thereby generating impact maps. A parameter score map reports maximum, minimum, and average scores;

(c) transformation of the impact maps into risk maps, followed by integration of these partial maps into a comprehensive risk map.

This study reproduces these steps, presenting both the site-specific input parameters and the outputs of each stage, commencing with the evaluation of the key factors and impact table developed for salt caverns (H_2 storage) by Anzelmo et al. [34] and the creation of a site card specific to the Realmonte site. The scores and results of the maps were contingent upon the values attributed to each parameter and the impact values assigned according to the ranges considered based on the literature review.

The selected parameters are:

- **Geological parameters:** top salt depth, salt lithology, salt thickness, fault occurrence, caprock integrity, and caprock thickness.
- **Rock salt parameters:** structural complexity, salt interlayer frequency, salt interlayer lithology, salt deposition conformation, insoluble sulfates, and salt anomalies.
- **Environmental parameters:** seismic hazard, location, water availability, proximity to wells and/or productive areas, urban/rural areas, natural protected areas and rivers, infrastructure, and brine management.

The workflow was applied separately for the lower portion of the site from approximately -250 m below sea level (here called "First Cycle") to the upper portion (here "Second Cycle") above -250 m that includes the sector currently occupied by the active Realmonte mine.

3.1 Site card and Parameter Score Chart for the “First Cycle” at the Realmonte site

The site card in Table 1 shows the parameters with their assigned values and corresponding impact values (-3 to +3), the latter assigned based on the ranges chosen from the impact table given by Anzelmo et al. [34].

The first column presents the individual parameters selected from the key-factor table. The second column displays the actual values corresponding to the site, derived from the dataset available for the Realmonte site, which, in this specific instance, comprises approximately 40 boreholes reaching depths of up to 900 m along with the corresponding 3D geological model. The third column shows the average impact value assigned to each parameter. The fourth column indicates the robustness of the parameter type considered, which represents the reliability of the data source in column 2. The three columns “score”, “robustness”, and “score robustness”, contain the calculation of the product between each IMPACT and WEIGHT in the key factor table (score). The robustness score for each parameter is automatically retrieved using a conditional formula (IFS, multiple IF statements) that aligns the selected option (parameter robustness for the field column) with the corresponding category in the robustness table (key factors table). The score is then assigned based on the header value (row 5) of the matching column. Subsequently, the column product of ROBUSTNESS and WEIGHT from the key factor table yields a robustness score. Additionally, the total score and robustness are provided on the margin of the table.
Each parameter in the site card receives a partial score computed as:

$$\mathbf{S_i = w_i \times I_i} \qquad (1)$$

where w_i is the weight assigned to parameter i (ranging from 1 to 3, reflecting its relative importance for salt cavern gas storage suitability) and I_i is the impact value (ranging from -3 to +3, reflecting the site-specific geological or environmental condition for that parameter). The total raw score is the sum of all partial scores:

$$\mathbf{S_{raw} = \Sigma S_i = \Sigma(w_i \times I_i)} \qquad (2)$$

To express the total score on a normalised 0-100 scale, the following formula is used:

$$\mathbf{S_{norm} = [(Sraw - Smin) / (Smax - Smin)] \times 100} \qquad (3)$$

where *Smax* and *Smin* are derived from the key-factor table. Specifically, *Smax* is the sum of each parameter weight multiplied by its maximum achievable positive impact, and *Smin* is the sum of each parameter weight multiplied by its maximum achievable negative impact. These values are not simply symmetric ($\pm\Sigma w_i \times 3$), because some parameters (e.g., caprock thickness, seismic hazard, location, wells/productive areas distance) have asymmetric impact ranges: their maximum positive impact is limited to +1, whereas their negative impact can extend to -2 or -3. With the calibrated weights (range 1-3) applied to the 20 parameters retained in this study, *Smax* = 89 and *Smin* = -102.

The total robustness is computed analogously:

$$\mathbf{R_{norm} = [(Rraw - Rmin) / (Rmax - Rmin)] \times 100} \qquad (4)$$

where Rraw is the sum of all parameter score robustness values ($w_i \times I_i \times robustness_i$), and R_max and R_min are the theoretical bounds derived from the key-factor table. The robustness value quantifies the reliability of the data source used to assign the impact. A six-class scale from -2 to +3 is adopted, with each class mapped to a perturbation range ε for the Monte Carlo sensitivity analysis:

Table 1. Six-class robustness scale (−2 to +3) with perturbation ranges (ε) for the Monte Carlo sensitivity analysis.

Robustness	Data quality	ε (MC range)	Example sources
+3	Excellent: direct operational validation from decades of continuous service	±3%	Operational cavern monitoring, >10 yr cycling data, solution mining records
+2	Good: direct measurement with adequate spatial coverage	±5%	Well logs, core analysis, dense borehole grids, laboratory tests
+1	Moderate: indirect but reliable evidence	±8%	Seismic interpretation, geological model, limited published data
0	Low: no site-specific data; default assumption	±12%	Literature values, regional averages, analogy from similar formations
−1	Poor: sparse or uncertain data	±18%	Single borehole extrapolation, incomplete logs, old regional studies
−2	Very poor: essentially unknown	±25%	Analogy from distant sites, expert opinion without supporting data

The +3 class applies to parameters at sites with long operational track records. At Teesside (>50 years of continuous H_2 storage) and Clemens Dome (>40 years, >60000 pressure cycles), the majority of geological and rock salt parameters have been validated by decades of successful operation, providing a level of data confidence that exceeds direct measurement. For Realmonte, which is at the pre-feasibility stage with no operational history, the maximum achievable robustness is +2 (±5%), constrained by the ~40 borehole coverage from the 1970s mining campaign. This distinction ensures that the Monte Carlo perturbation ranges reflect the actual information gap between operational and pre-feasibility sites.

Weights reflect the relative importance of each parameter for the suitability of a salt formation for cavern gas storage: they are site-invariant constants, derived from published literature and expert assessment, and remain identical across all sites evaluated with this methodology. Impact values, by contrast, are site-specific variables determined by the actual geological, rock salt, and environmental conditions at each site.

Robustness values are also site-specific, determined by the quality and availability of data for each parameter at the site under evaluation. This distinction is fundamental: the CRS total score is driven primarily by site-specific impacts (which reflect geology) rather than by operator-dependent weight choices.

3.2 Sensitivity Analysis

To assess the stability and robustness of the CRS scoring system, a Monte Carlo (MC) sensitivity analysis was performed on the weight-by-impact perturbation space. For each of the 500 MC simulation runs, the partial score of each parameter was perturbed by a random factor drawn from a uniform distribution within a range ε defined by the parameter's robustness class:

Table 2. Five-class robustness scale (−2 to +2) applied to the Realmonte site cards.

Robustness class	Data quality	ε (perturbation range)
+2	Direct measurement (well data, core)	±5%
+1	Indirect reliable evidence (seismic)	±8%
0	No specific data	±12%
−1	Sparse or uncertain data	±18%
−2	Extrapolated or assumed values	±25%

This calibration ensures that parameters supported by high-quality data (e.g., direct well measurements, +2 robustness) experience minimal perturbation, while parameters with poor data support are subject to wider variation. For each MC run, the perturbed partial scores are summed and normalised using Equation (3) to obtain a perturbed total score. The MC output consists of 500 normalised total scores, from which the mean, standard deviation (SD), and coefficient of variation (CV) are computed. A CV below 1% indicates that the ranking is highly stable under data uncertainty. The sensitivity analysis was applied to both Realmonte sections and to two international benchmark sites (Teesside, UK; Clemens Dome, USA) to validate the cross-site stability of the methodology (see Part 1 for full details).

An important outcome of the sensitivity calibration is the restriction of parameter weights to the range 1-3, rather than adopting a wider range such as 1-5 or 1-10. Monte Carlo simulations showed that wider weight ranges introduced instability in the total score, with the CV increasing significantly and ranking reversals occurring between sites. Constraining the weights to 1-3 stabilises the MC output (CV $< 0.3\%$ for all tested sites) and ensures that the total score is controlled mainly by site-specific impact values, which reflect actual geology, rather than by subjective weight assignments. This calibration represents a key methodological contribution of the CRS approach.

4. Results

This section presents the results for the two sections of the site. The lower section is described first, as it is considered the more promising target and extends beneath the active mining area. This is followed by the results for the upper section, which includes the mine itself and whose presence was incorporated among the environmental parameters.

4.1 Site card and Parameter Score Chart for the First Cycle

The site card for the First Cycle (Table 3) integrates all 20 geological, rock salt, and environmental parameters with their site-specific values, impact scores, weights, and robustness assignments. Impact values were assigned according to the ranges defined in the key-factor table [34], based on the dataset

available for the Realmonte site, which comprises approximately 40 boreholes reaching depths of up to 500 m, supplemented by mine-level geological observations and three-dimensional geological modelling.
The normalised total score for the First Cycle is 95.81%, reflecting highly favourable geological conditions: pure halite at optimal depth (below -250 m), salt thickness exceeding 200 m, absence of significant faulting, and strong caprock integrity. The total robustness is 77.36%, indicating high data reliability supported by the dense borehole coverage from the 1970s mining exploration campaign. The most influential positive contributors are top salt depth, salt lithology, and fault occurrence (each scoring the maximum partial score of +9), while the only mildly penalising parameter is infrastructure proximity due to the active mine operating at shallower levels.

Table 3. Site card for the First Cycle at the Realmonte site (normalised CRS score = 95.81%).

Parameter	Value	Impact (−3/+3)	Data source	Score	Robust.	Score Rob.
GEOLOGICAL PARAMETERS						
Top salt depth (m)	450	3	Well data (~40 boreholes)	9	+2	−20
Salt lithology	Pure halite	3	Well data	6	+2	10
Salt thickness (m)	300	2	Well data	4	+2	4
Caprock integrity	No faults / long distance migration path	3	3D geological model	9	+2	6
Caprock thickness	>75% of cavern diameter	1*	3D geological model	3	+2	6
Fault occurrence	No faults	3	3D geological model	9	+2	4
ROCK SALT PARAMETERS						
Structural complexity	No active deformation	3	3D geological model	6	+2	4
Interlayer frequency	Thick interlayers (avg. 2 m)	3	Well data	6	+2	0
Interlayer lithology	No interlayer lithology	1	Well data	1	+2	4
Deposit conformation	Layered salt without deformation	3	3D geological model	3	+2	2
Insoluble sulfates (%)	0	3	Well data	6	+2	4
Salt anomalies	Salt grain variation with anhydrite	1	Well data	1	−2	−4
ENVIRONMENTAL PARAMETERS						
Seismic hazard (PGA)	< 0.1 g	1*	Maps	2	−1	−4
Location (On/Offshore)	Onshore	1*	Maps	2	+2	8
Water availability	Natural basin / river	3	Maps	3	+2	6
Wells / productive areas	Distance > 3× cavern diameter	1*	Maps	1	+2	6
Urban / rural area	No urban area	3	Maps	3	+2	6
Natural protected areas & rivers	No natural protected area	3	Maps	3	+2	6
Infrastructure	No infrastructure	3	Maps	3	+2	6
Brine management	Direct discharge into sea	1	Maps	1	−1	−3
TOTAL SCORE (normalised): 95.81% | TOTAL ROBUSTNESS: 77.36%				**81**	**74.06%**	

Figure 2 shows a parameter score chart that graphically illustrates the trend of total score values in comparison with the minimum and maximum scores for each parameter under consideration. Notably, the top salt depth parameter and lithology, characterized by pure halite at those depths at the site, make a significantly favorable contribution.

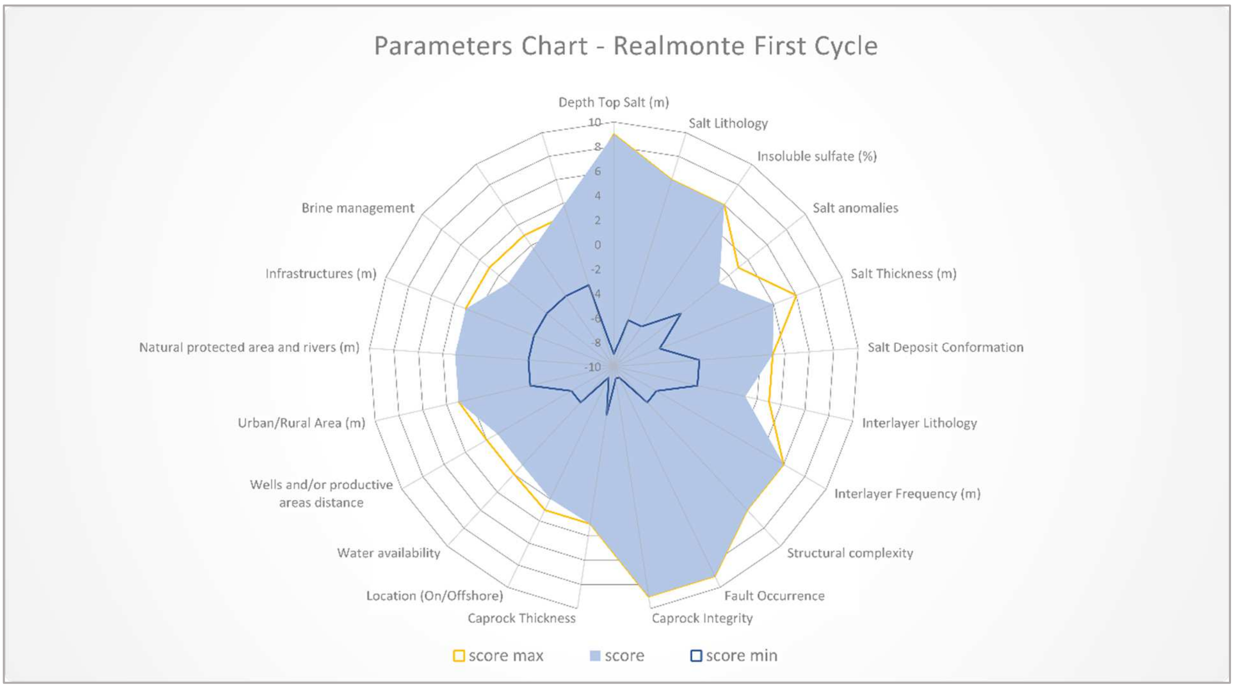

Fig. 2 Parameter chart for the lower section of the Realmonte site

4.1.1 Generation of impact maps and risk assessment based on the CRS approach- First Cycle

The impact maps were generated by extrapolating surfaces from the geological model and converting them into polygonal maps. These were then reprocessed for each site card parameter and reclassified into impact maps based on qualitative storage suitability, with the assignment of a chance value and colour corresponding to the impact of each area, thus producing the corresponding CRS maps (Figs. 3a, b, and c). The CRS maps were subsequently integrated using a GIS function that overlays multiple maps and multiplies the risk values of each polygon in the input layers. For example, the geological risk map was obtained by multiplying the following maps: Top Salt Map, Salt Lithology Map, Salt Thickness Map, Fault Occurrence Map, Caprock Integrity Map, and Caprock Thickness Map (Fig.3). In this way, three partial risk maps were generated (CRS Geology Map, CRS Salt Properties Map, CRS Environmental Map; Fig. 4), which can be analysed separately or combined in a final step to obtain the overall risk map (Fig. 5A, B, and C).

In Fig. 5, the difference between maps B and C is particularly noteworthy. Map B shows the final CRS map, in which the combined contribution of all individual maps produces a more critical scenario in the central part of the site, reflected by higher storage risk values. By contrast, map C was produced by inputting the score values from the site card into the GIS. A comparison of the two maps clearly shows that the site-card score map yields significantly more optimistic results. For safe storage assessment, the final CRS map was considered the most appropriate.

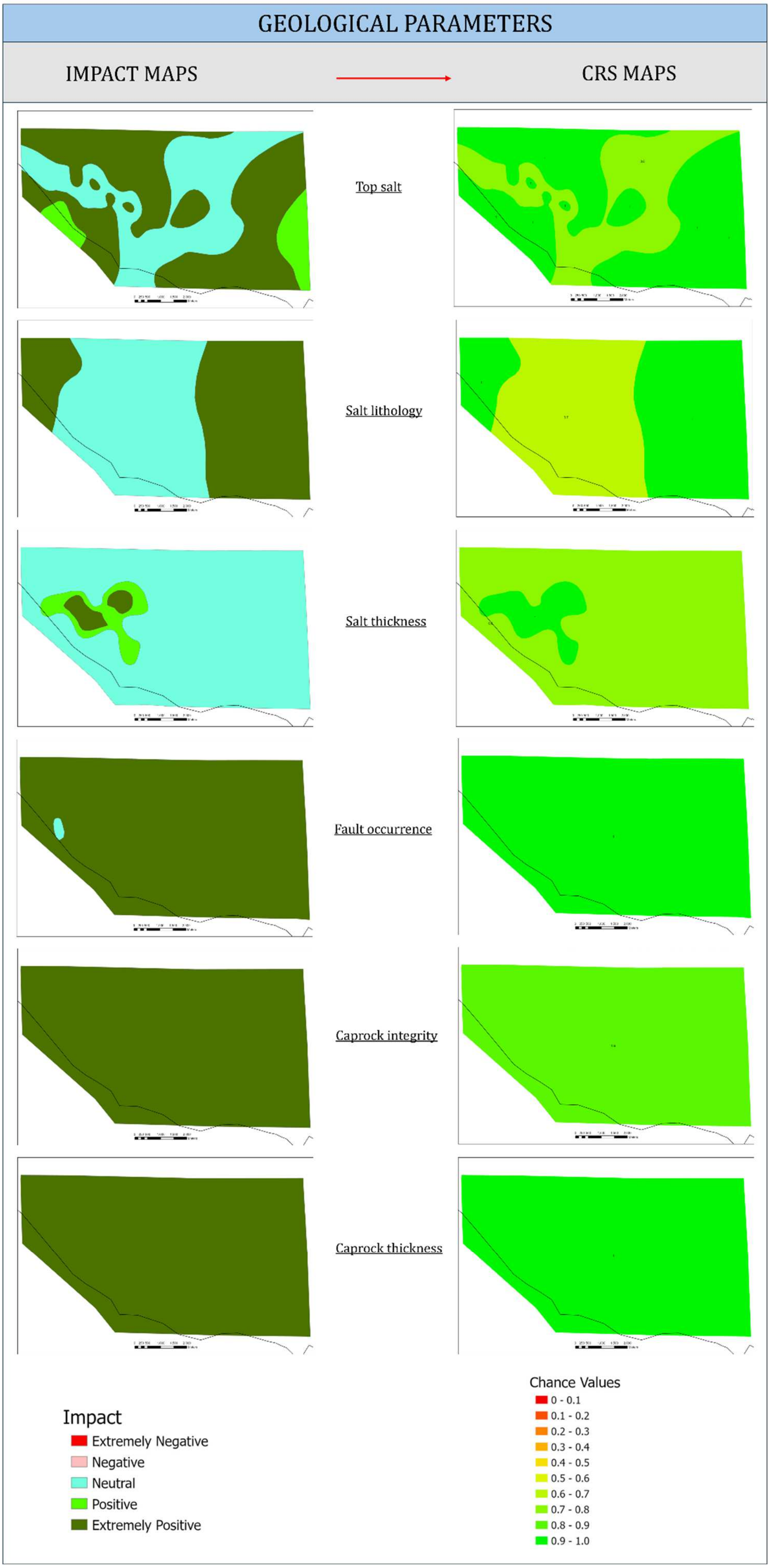

Fig. 3 a) Scheme for converting impact maps into CRS maps. The maps were derived from polygon maps related to geological parameters.

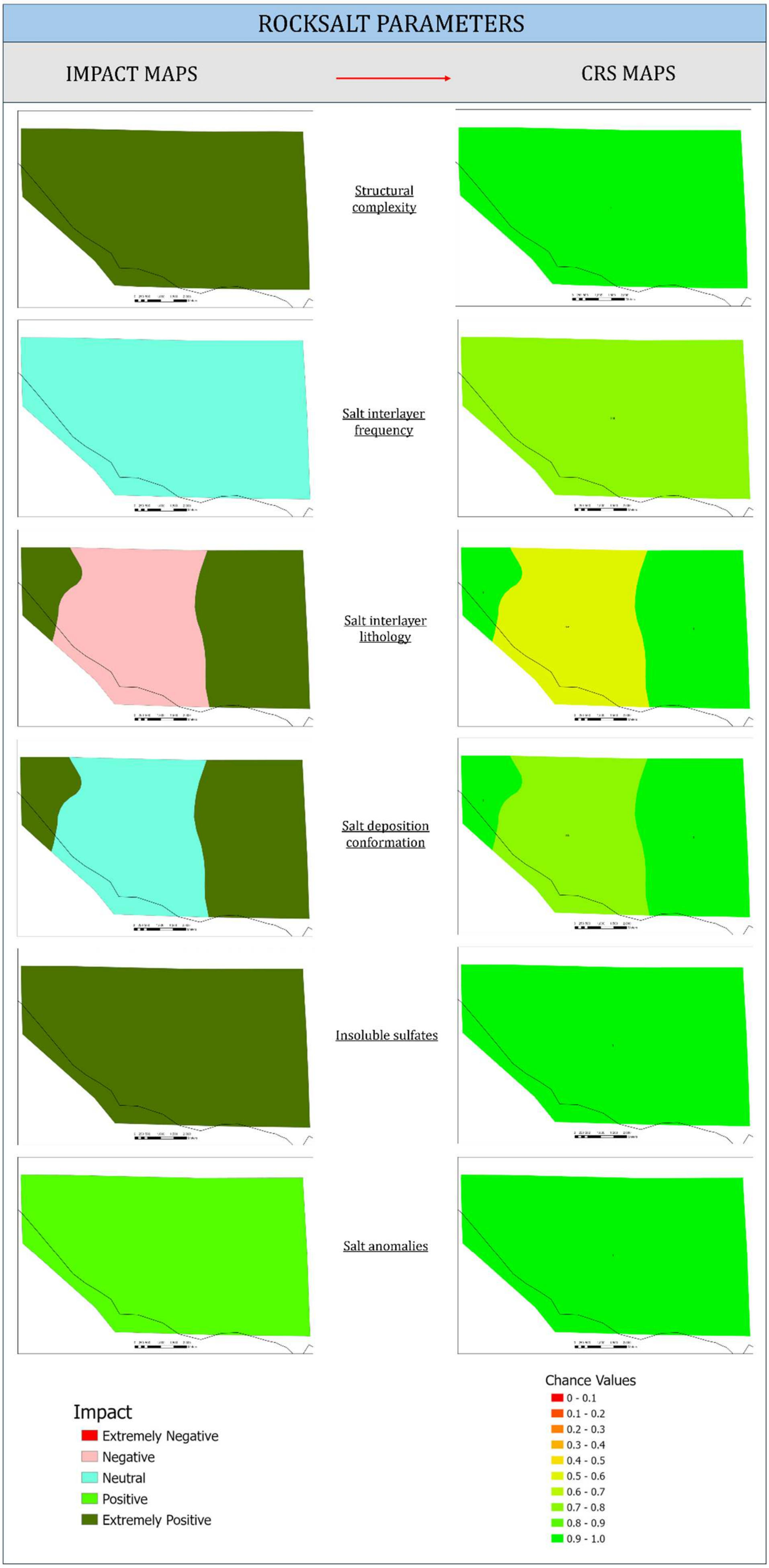

Fig. 3 b) Scheme for the conversion of impact maps to CRS maps. The maps were derived from polygon maps related to the rock salt parameters.

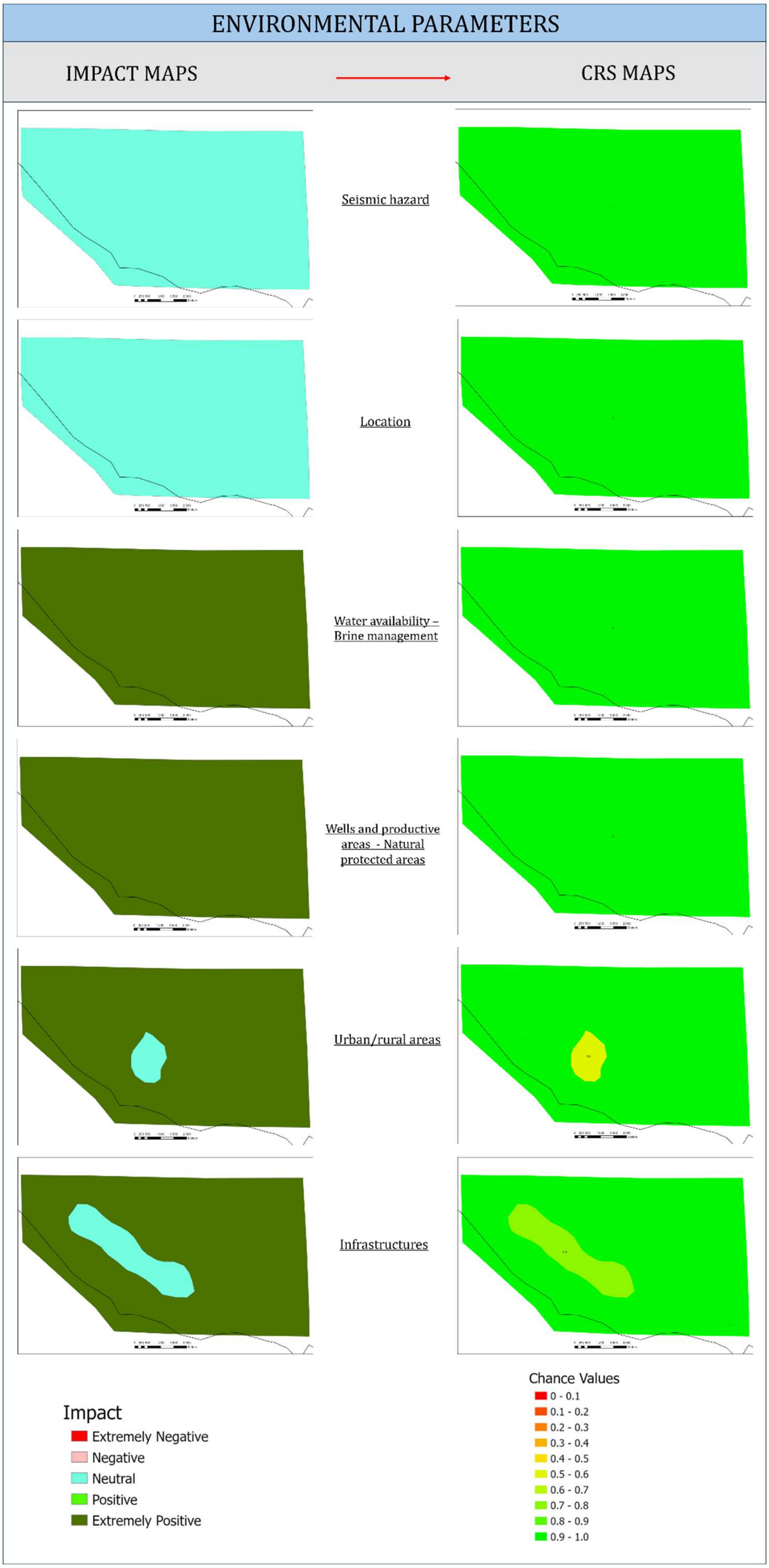

Fig. 3 c) Scheme for converting impact maps to CRS maps. The maps were derived from polygon maps related to the environmental parameters.

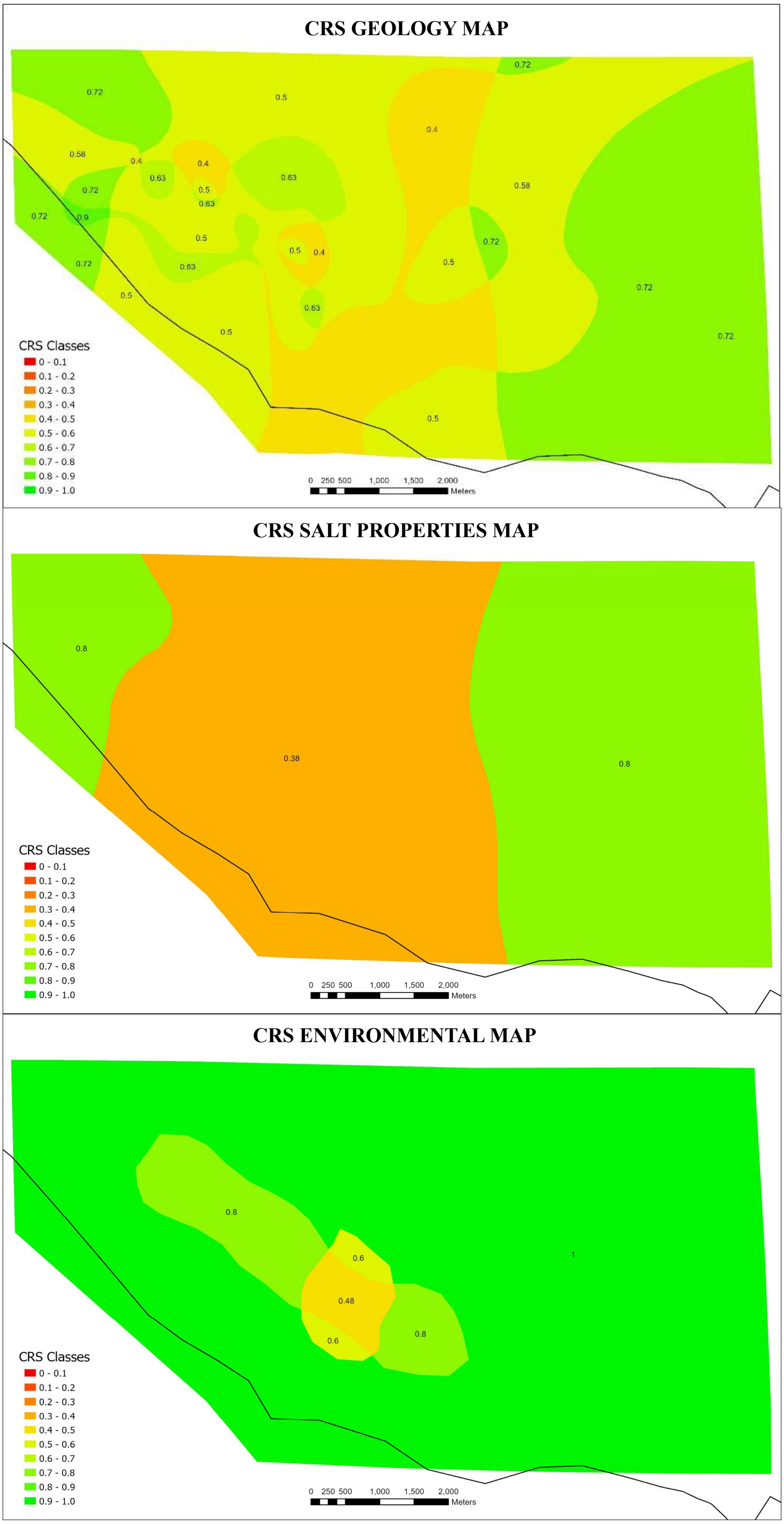

Fig. 4 Partial CRS maps obtained by multiplicative combination in GIS of the CRS maps related to each parameter for the first salt cycle

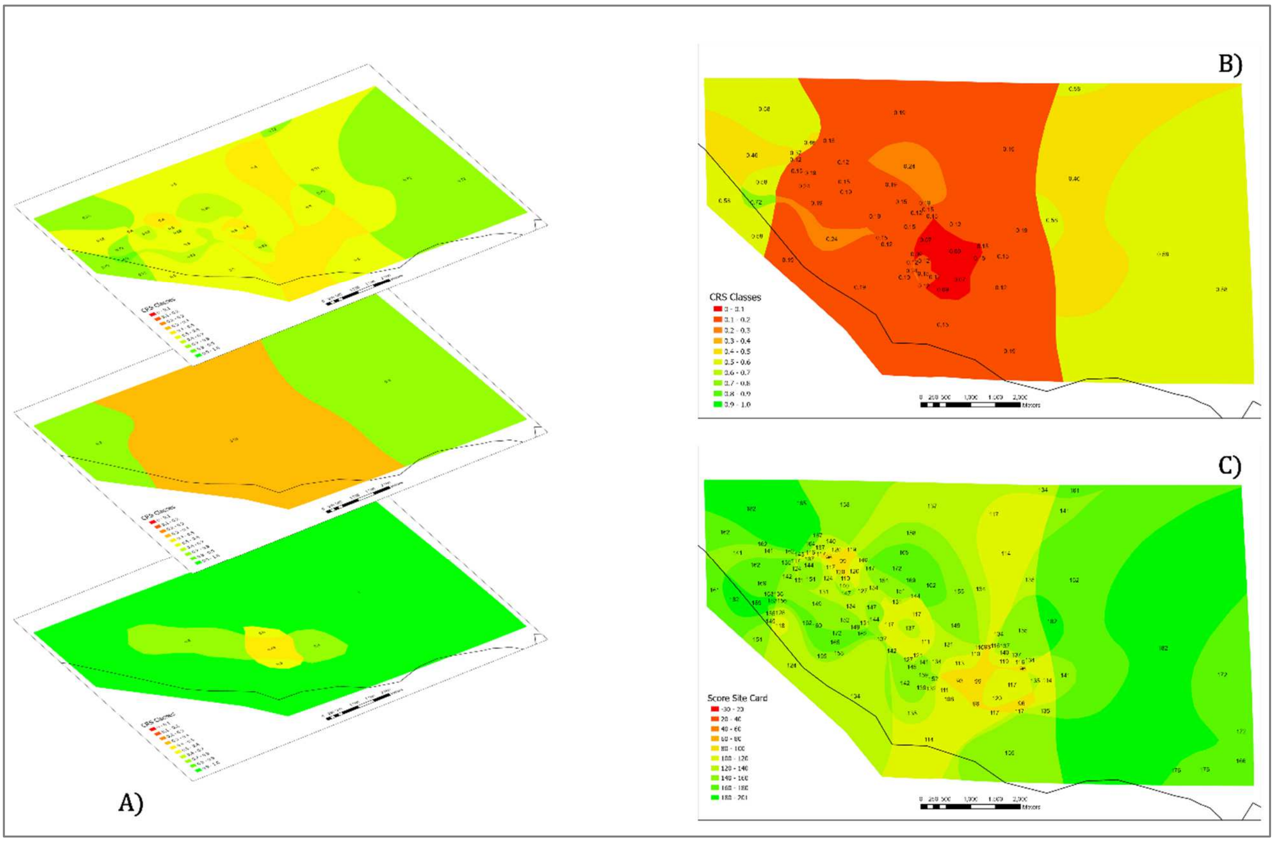

Fig. 5 The figure illustrates the process by which the integration of the three maps (Fig. 4) CRS partials: (A) results in the final CRS map (B). This final map is subsequently compared with the site card map (C), which is regarded as yielding more optimistic results.

4.2 Site card and Parameter Score Chart for the "Second Cycle" at the Realmonte site

Table 4 presents the site card developed for the upper section of the Realmonte site. In this context, several geological parameter values are notably negative, reflecting the less favourable characteristics of the shallow salt section. The total raw score is 64, corresponding to a normalised score of 86.91% (Equation 3). While lower than the First Cycle, this score still indicates a site with generally positive attributes. The total robustness remained acceptable at 60.38%. The Monte Carlo sensitivity analysis yields a mean normalised score of 86.91% with SD = 0.14 and CV = 0.16%. However, as discussed in Section 5, the presence of the active Realmonte mine in the Second Cycle creates a fundamental operational incompatibility with hydrogen storage that cannot be captured by the CRS score alone.

Table 4. Site card for the Second Cycle at the Realmonte site (normalised CRS score = 86.91%).

Parameter	Value	Impact (−3/+3)	Data source	Score	Robust.	Score Rob.
GEOLOGICAL PARAMETERS						
Top salt depth (m)	< 200	1	Well data	3	-2	-20
Salt lithology	Halite + thick Mg-K salt layers	2	Well data	4	-2	-10
Salt thickness (m)	150	2	Well data	4	-2	-4
Caprock integrity	Moderate (thin overburden)	2	Well data	6	+2	6
Caprock thickness	<75% of cavern diameter	1*	3D geological model	3	+2	6
Fault occurrence	No faults	3	3D geological model	9	+2	4
ROCK SALT PARAMETERS						
Structural complexity	No active deformation	3	3D geological model	6	+2	4
Interlayer frequency	High number, very thin interlayers	3	Well data	6	+2	0
Interlayer lithology	Gypsum, Mg-K salt, insoluble sulfate	2	Well data	2	+2	4
Deposit conformation	Diapiric with low heterogeneity / layered	2	3D geological model	2	+2	2
Insoluble sulfates (%)	30	2	Well data	4	-2	-4
Salt anomalies	Strings, bands, BSZ with gas pockets	1	Well data	1	-2	-4
ENVIRONMENTAL PARAMETERS						
Seismic hazard (PGA)	< 0.1 g	1*	No data	2	-1	-4
Location (On/Offshore)	Onshore	1*	Maps	2	+2	8
Water availability	Natural basin / river	3	Maps	3	+2	6
Wells / productive areas	< 2-3× cavern diameter	1*	Maps	1	+2	6
Urban / rural area	~2000 m	1	Maps	1	+2	6
Natural protected areas & rivers	No natural protected area	1	Maps	1	+2	6
Infrastructure	Salt mine present	1	Maps	1	+2	6
Brine management	Direct discharge into sea	3	No data	3	-1	-3
TOTAL SCORE: Raw = 64 | Normalised = 86.91% | TOTAL ROBUSTNESS = 57.08%						

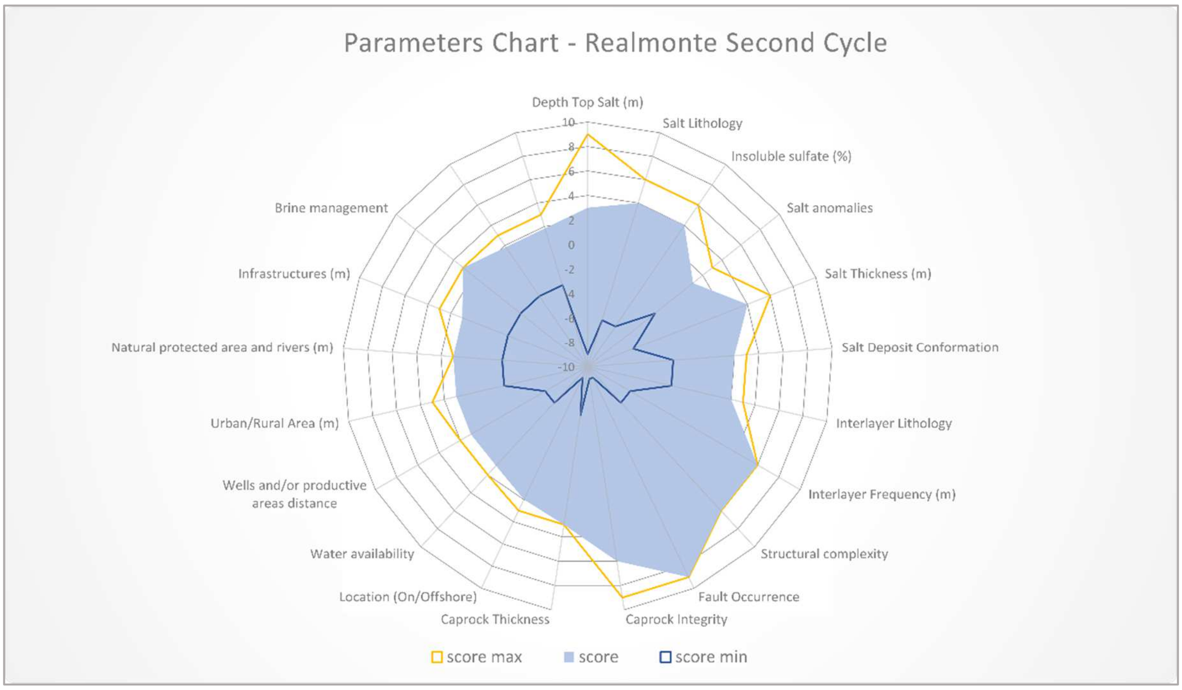

Fig. 6 Parameters chart for the upper section of the Realmonte site

4.3 Generation of impact maps and risk assessment based on the CRS approach - Second Cycle

Because the same workflow was applied to the lower section, only the final outputs from the combinations of the CRS maps are presented here for the upper section. These include the partial risk maps corresponding to the three parameter groups (geological, rock salt, and environmental; Fig. 7), as well as their integration into the final comprehensive risk map for the saline sequence extending from approximately -250 m b.s.l. to the surface (Fig. 8).
As shown in Fig. 7, the geological parameters exhibited the greatest sensitivity (and consequently exerted the most significant influence on the algorithm), as previously indicated by the corresponding site card. The shallow depth of the salt top, coupled with the insufficient thickness of the usable salt, resulted in at least 80 percent of the map being classified as zero (indicating very high risk). Acceptable CRS values were derived from the map of factors related to the properties of rock salt in this section, suggesting that if these factors were considered in isolation, the potential of the site for rock salt quality would remain of interest. Conversely, the CRS map of environmental parameters indicates that, theoretically, the only restricted area would be confined to the current extent of the active mine, with the potential remaining high (low risk) in all surrounding areas.
Figure 8 shows the final CRS map, which integrates the geology, salt properties, and environmental maps. The result is markedly pessimistic, with near-zero values largely driven by the geological factor map. As in the lower sequence, the site-card score map appears more optimistic because it preserves the individual contribution of each parameter considered separately.

4.4 Sensitivity Analysis Results

The Monte Carlo sensitivity analysis described in Section 3.2 was applied independently to both stratigraphic sections of the Realmonte site and to two operational benchmark sites (Teesside, UK, and Clemens Dome, USA) to validate the scoring framework.

*First Cycle***.** The MC simulation for the Realmonte First Cycle yields a mean normalised score of 95.81% with a standard deviation of 0.13% and a coefficient of variation (CV) of 0.14%. The narrow uncertainty envelope (range: 95.55-96.07%) reflects the high overall robustness of this section (+2 for the majority of geological and rock salt parameters), supported by the dense borehole coverage (~40 wells) from the 1970s mining exploration campaign. The only parameter contributing appreciable uncertainty is salt anomalies (robustness -2, $\varepsilon = \pm 25\%$), as no systematic anomaly testing (e.g., ultrasonic scanning or sonar surveys) has been performed at Realmonte. Despite this, the perturbation of a single low-robustness parameter does not alter the total score significantly, confirming that the First Cycle assessment is robust and data-driven.

*Second Cycle***.** The MC simulation for the Second Cycle yields a mean normalised score of 86.91% with a standard deviation of 0.14% and a CV of 0.16%, marginally higher than the First Cycle. The slightly wider uncertainty reflects the lower overall robustness of this section: several geological parameters (top salt depth, salt lithology, salt thickness, insoluble sulfates, salt anomalies) carry robustness values of -2 ($\varepsilon = \pm 25\%$), consistent with the greater geological heterogeneity and reduced data confidence in the shallower portion of the sequence. Nevertheless, the CV remains well below 1%, indicating that the Second Cycle score is stable and the gap with the First Cycle ($\Delta = 8.90$ percentage points) is statistically significant and preserved in 100% of MC runs.

Cross-site ranking. To place the Realmonte scores in context, the same MC framework was applied to Teesside (UK, operational since 1972) and Clemens Dome (USA, operational since 1983). Site cards for these benchmark sites were constructed from published geological, operational, and environmental data using the same key-factor table. Table 5 summarises the results for all four site configurations.

Table 5. Cross-site Monte Carlo sensitivity results (N = 500 runs). Ranking preserved in 100% of runs.

Site	Raw score	Normalised (%)	MC mean (%)	SD	CV (%)	Rank
Realmonte 1st Cycle	81	95.81	95.81	0.13	0.14	1st
Clemens Dome (USA)	73	91.62	91.62	0.11	0.12	2nd
Realmonte 2nd Cycle	64	86.91	86.91	0.14	0.16	3rd
Teesside (UK)	60	84.82	84.82	0.21	0.26	4th

The ranking order, Realmonte First Cycle (95.81%) > Clemens Dome (91.62%) > Realmonte Second Cycle (86.91%) > Teesside (84.82%), is preserved in 100% of the 500 MC runs across all four sites. The minimum pairwise gap (Realmonte Second Cycle vs Teesside, Δ = 2.09 percentage points) exceeds the combined standard deviations by an order of magnitude, confirming that the ranking reflects genuine geological differences rather than scoring noise.

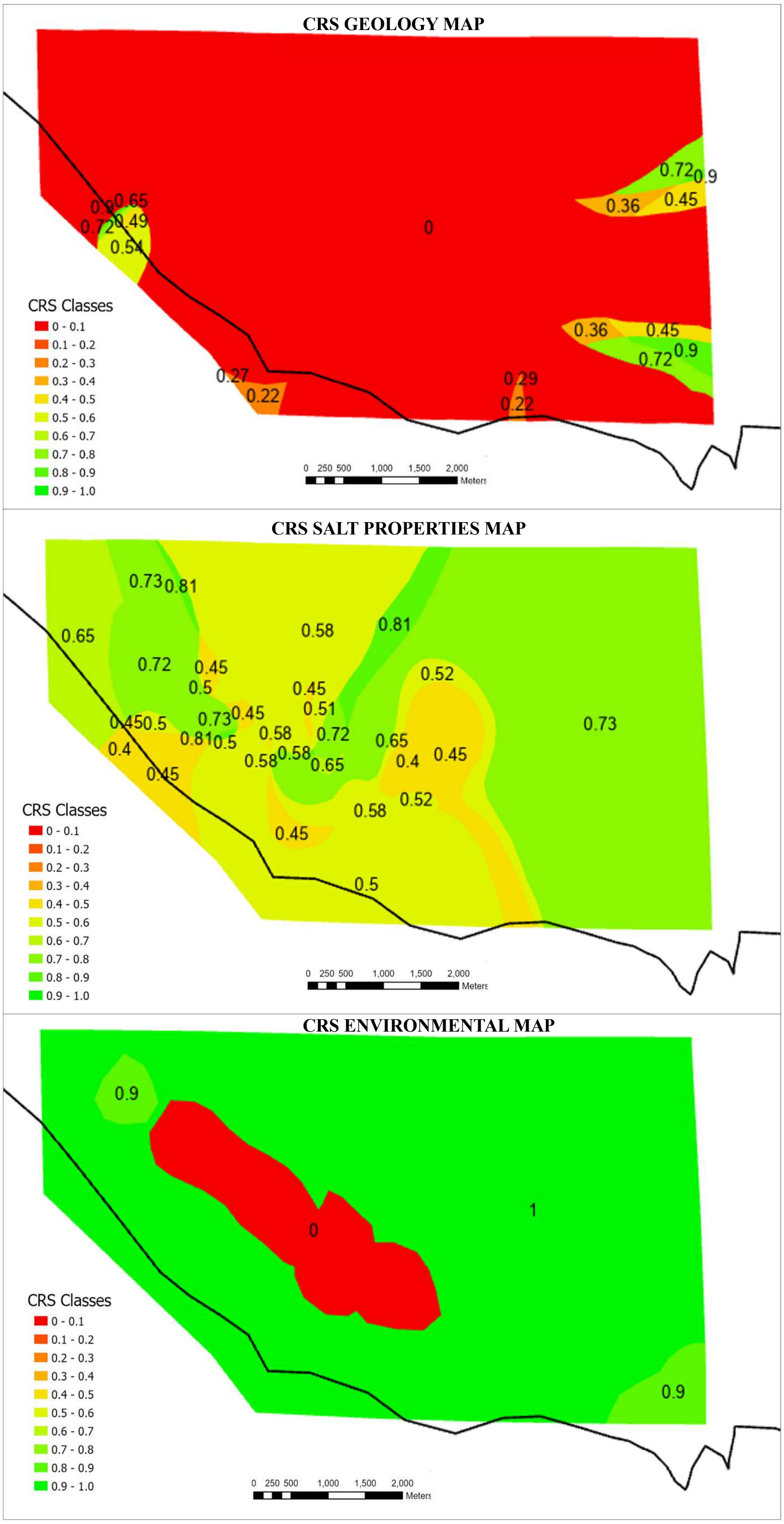

Fig. 7 Partial CRS maps obtained by multiplicative combination in GIS of the CRS maps related to each parameter for the second salt cycle.

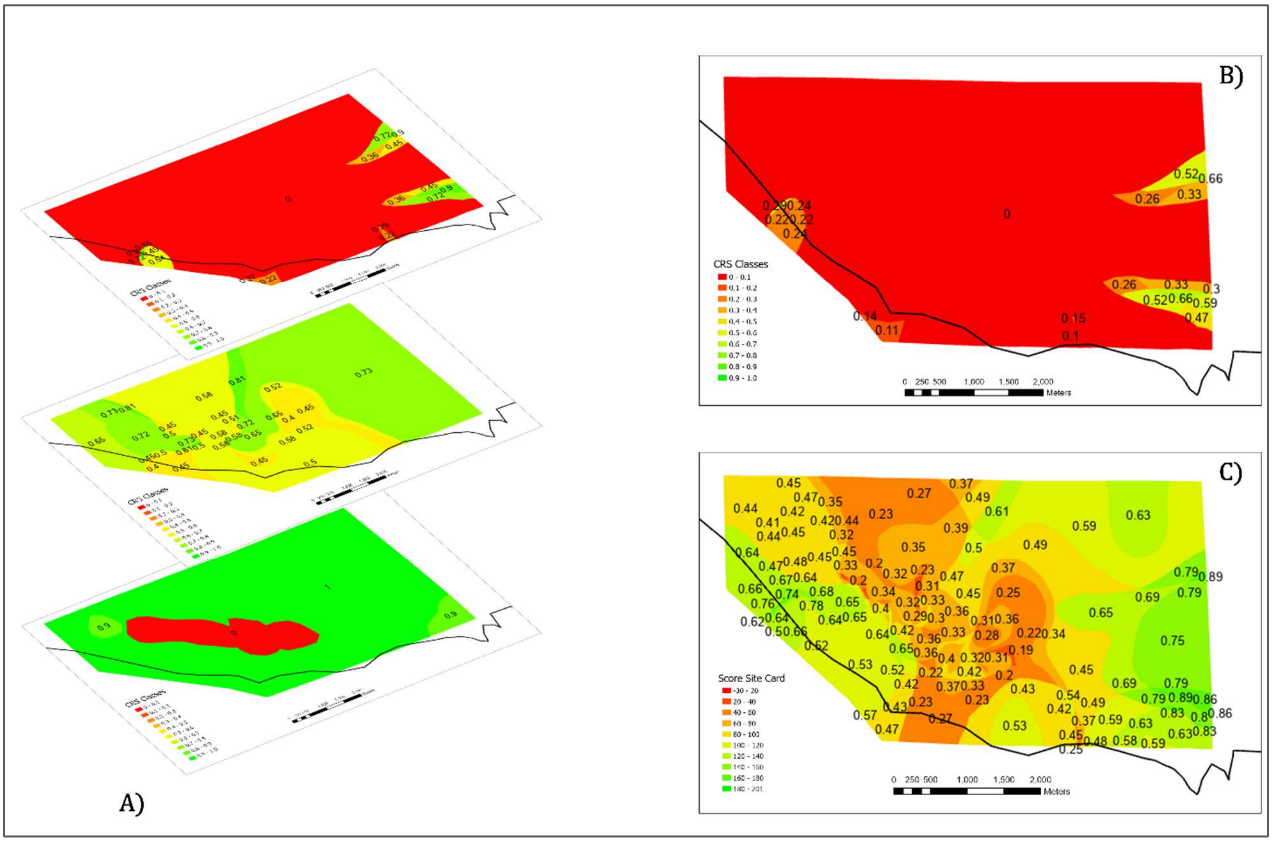

Fig. 8 The figure shows the process by which the integration of the three maps CRS partials: (A) results in the final CRS map (B). This final map is subsequently compared with the site card map (C), which is regarded as yielding more optimistic results too here in the second cycle.

5. Discussions

5.1 Realmonte First cycle

The values of each parameter were directly extrapolated from the available deep borehole data and the three-dimensional geological model of Realmonte. The salt sequence extending below the current active mine, at depths exceeding approximately -250 meters, exhibits features of significant interest regarding its potential for hydrogen storage. The depth of the salt top, attributed to the cumulative thickness of the overburden deposits (comprising gypsum and Plio-Pleistocene deposits) and the upper salt sequence, which in the depocenter reaches up to 500 meters, supports the storage potential in terms of safety. This, combined with the favorable parameters of caprock integrity and thickness, also enhances seal capacity. As reported in Section 4.1, the First Cycle achieves a normalised score of 95.81% with high robustness (77.36%), driven by the favourable geological conditions of the deep salt section. Beyond the parameters captured by the CRS scoring, the site offers additional logistical and geological advantages discussed below.

The Realmonte benefits from logistical conditions that further strengthen its suitability. Its coastal location provides direct access to seawater for solution mining and natural pathways for brine disposal, eliminating the need for expensive inland brine management infrastructure. Proximity to planned offshore renewable energy hubs, including the Med Wind floating wind farm (~80 km offshore) and several onshore wind farms in the Agrigento province, positions Realmonte as a strategic node in Sicily's emerging hydrogen value chain. Furthermore, the existing mining infrastructure (roads, power supply, port access) reduces the capital expenditure required for initial site development. Seismic hazard at Realmonte is very low (PGA < 0.1 g), consistent with the regional seismotectonic setting of southern Sicily. The site is located within a zone of low to moderate seismicity, remote from the active tectonic structures of the Calabrian Arc and the Etna volcanic complex. This low seismic exposure, combined with the absence of significant faulting within the salt sequence, ensures favourable conditions for long-term cavern integrity and operational safety.

Caprock integrity at the Realmonte site was from the stratigraphic and structural characteristics visible in the borehole dataset and the 3D geological model. Above the First Cycle, the caprock consists of a thick sequence of marly clays and gypsum belonging to the Upper Evaporite unit, forming a laterally continuous seal. The absence of faults intersecting this interval, as confirmed by the structural model, supports the assignment of a high positive impact (+3) for caprock integrity in the site card. No legacy wells or abandoned boreholes are known to penetrate the target salt interval below -250 m, removing a major potential leakage pathway. Nevertheless, a detailed geomechanical assessment of caprock mechanical properties (e.g., tensile strength, fracture toughness) and potential failure pathways would still be required during a later feasibility phase.

All environmental parameters of the CRS site card all receive positive impact values for the First Cycle, confirming that no environmental constraint limits the storage potential. The site does not fall within any Natura 2000 protected area; the nearest designated site (ITA040015, Torre Salsa) is located at a distance exceeding the regulatory buffer. Water availability is ensured by the coastal location, and the distance from urban centres and existing wells exceeds the minimum safety thresholds defined in the key-factor table. Brine management, assigned an impact of +1, benefits from the offshore discharge option, although a detailed environmental impact assessment for brine disposal would be required at the permitting stage. The borehole dataset underpinning the Realmonte 3D geological model dates from the 1970s mining exploration campaign and no modern geophysical surveys (e.g., 3D seismic reflection) have been acquired to date. While the robustness framework captures this data limitation through reduced robustness scores (and correspondingly wider Monte Carlo perturbation ranges), the authors recommend that any future site development programme includes a dedicated geophysical verification campaign to refine the structural model, constrain interlayer frequency and halite purity at depth, and improve robustness from the current +2 level toward the +3 class achieved at operational sites.

5.2 Realmonte Second cycle

For the second cycle, the site card reflects the characteristics of the shallower part of the deposit. The cover above the salt succession reaches a maximum thickness of approximately 180 m. Although the salt unit immediately beneath is of excellent mining quality, it has been exploited for alkali salts since the late 1980s and lacks the requisite capacity for potential storage applications (impacts -2 and -3 of Table 2). Furthermore, in the upper section of the Realmonte site, which is affected by mining activities (Fig. 1b), there are several interlayers of magnesium and potassium salts, primarily kainite and other potassic salts, which exhibit greater solubility than halite. Even without the presence of the mine, this would entail the need for careful management of the leaching phase. Additionally, there are a couple of insoluble layers approximately 3-4 meters thick. These features significantly diminish the suitability of the site at this level, thereby increasing the risk factors.

Although rocksalt parameters are not unfavorable, their potential is substantially compromised by geological factors. A similar rationale applies to the impact values related to environmental factors, which remain highly favorable for the site for the reasons previously discussed. In terms of evaluating structural parameters, the considerations made for the first cycle remain applicable, as they do not significantly influence the overall score, which is more than half of the score of the lower salt sequence.
When evaluating the hypothetical potential for hydrogen storage, it becomes evident that a deeper sequence is preferable, while a shallower sequence should be avoided for the reasons previously discussed also for this specific site. Although the Second Cycle presents very favourable environmental conditions, comparable to those of the First Cycle, its development for hydrogen storage is precluded by two independent and equally critical constraints. First, the geological setting is fundamentally inadequate: the top of salt lies at less than 200 m depth over much of the area, well below the minimum threshold required for reliable pressure containment, and caprock thickness is insufficient to guarantee long-term gas tightness at such shallow depths. These are hard geological constraints and cannot be engineered away. Second, the active Realmonte mine operates within the same stratigraphic interval, creating an operational incompatibility that would require stringent safety zoning and regulatory approvals without precedent in European mining law. Either constraint alone would be sufficient to exclude the Second Cycle from further consideration for hydrogen storage; together, they confirm that the First Cycle is the only viable target at the Realmonte site.

The proposed storage caverns in the First Cycle would be located at depths exceeding 400 m below sea level, while the active mine galleries operate down to approximately -200 m below sea level. The vertical separation between the mine floor and the top of the proposed cavern zone is therefore at least 200 m of continuous salt, well in excess of the minimum safety pillar thickness recommended in the literature (typically 2-3 times the cavern diameter, i.e., 120-240 m for the cavern dimensions considered here). Even so, the operational coexistence of mining and hydrogen storage within the same concession area would require a dedicated safety assessment addressing possible gas migration pathways and pressure monitoring protocols.

5.3 Cross-site benchmarking and ranking

Application of the CRS methodology to two internationally recognised hydrogen storage sites, Teesside (UK) and Clemens Dome (USA), provides a quantitative benchmark for the Realmonte results. Table 5 shows that the Realmonte First Cycle achieves the highest normalised CRS score (95.81%) among the four sites tested, surpassing Clemens Dome (91.62%) and Teesside (84.82%). This result is driven primarily by the exceptional geological characteristics of the lower Realmonte salt section: thick, pure halite at optimal depths (400-600 m), absence of faults, excellent caprock integrity, and low seismic hazard.
The fact that Realmonte First Cycle outscores two facilities with decades of operational history is both a validation of the CRS methodology and a significant result for the Italian hydrogen storage potential. Clemens Dome, despite its 40+ years of successful operation, receives a lower score because certain geological parameters (e.g., structural complexity associated with the diapiric setting, shallower top salt depth) are correctly penalised by the CRS scoring system. Teesside, while operationally proven, is penalised by its relatively thin bedded salt (<100 m), which limits cavern dimensions and contributes to a lower overall score.

It should be emphasized that the CRS score evaluates geological and environmental suitability at the pre-feasibility stage; operational factors such as infrastructure maturity, regulatory approvals, and market proximity are not captured. The Realmonte First Cycle, while geologically excellent, remains at the conceptual stage, whereas Teesside and Clemens Dome are mature operational facilities. Nevertheless, the cross-site ranking demonstrates that the CRS methodology can effectively discriminate between sites of varying geological quality and provides a reproducible, quantitative basis for site comparison.

The Monte Carlo analysis confirms that this ranking is not an artefact of weight assignment: the ranking is preserved in 100% of 500 simulation runs, with CV below 0.3% for all sites. The stability of the ranking under perturbation demonstrates that the CRS total score is driven by site-specific impact values, reflecting actual geology, rather than by operator-dependent weight choices, which is the intended design of the methodology.

The Realmonte Second Cycle (86.91%) ranks third, below Clemens Dome but above Teesside. However, as discussed in Section 5.2, the Second Cycle is excluded from further consideration on both geological and operational grounds. This underscores the importance of integrating the CRS quantitative assessment with qualitative operational and safety considerations in any final site evaluation.

Table 6. Robustness comparison: Teesside vs Realmonte (1st Cycle). ▲ = benchmark site has higher robustness than Realmonte; ▼ = lower; = equal.

Parameter	Impact	Weight	ε	Rob. Tees.	Rob. Realm.	Δ
Top salt depth	2	3	±3%	+3	+2	▲
Salt lithology	3	2	±3%	+3	+2	▲
Salt thickness	−2	2	±3%	+3	+2	▲
Caprock integrity	2	3	±3%	+3	+2	▲
Caprock thickness	−1	3	±8%	+1	+2	▼
Fault occurrence	3	3	±5%	+2	+2	=
Structural complexity	3	2	±3%	+3	+2	▲
Interlayer frequency	1	2	±5%	+2	+2	=
Interlayer lithology	1	1	±5%	+2	+2	=
Deposit conformation	2	1	±3%	+3	+2	▲
Insoluble sulfates	3	2	±3%	+3	+2	▲
Salt anomalies	2	1	±3%	+3	−2	▲▲▲
Seismic hazard	1	2	±5%	+2	+1	▲
Prox. wells/areas	1	1	±5%	+2	+1	▲
Urban/natural areas	1	2	±5%	+2	+1	▲
Infrastructure	3	1	±3%	+3	+1	▲▲
Brine management	3	1	±3%	+3	+1	▲▲
Water availability	3	1	±3%	+3	+1	▲▲
Location	1	2	±3%	+3	+2	▲

Table 7. Robustness comparison: Clemens Dome vs Realmonte (1st Cycle). ▲ = benchmark site has higher robustness than Realmonte; ▼ = lower; = equal.

Parameter	Impact	Weight	ε	Rob. Clem.	Rob. Realm.	Δ
Top salt depth	1	3	±3%	+3	+2	▲
Salt lithology	3	2	±3%	+3	+2	▲
Salt thickness	3	2	±3%	+3	+2	▲
Caprock integrity	3	3	±3%	+3	+2	▲
Caprock thickness	1	3	±5%	+2	+2	=
Fault occurrence	3	3	±3%	+3	+2	▲
Structural complexity	1	2	±5%	+2	+2	=
Interlayer frequency	3	2	±3%	+3	+2	▲
Interlayer lithology	3	1	±5%	+2	+2	=
Deposit conformation	1	1	±5%	+2	+2	=
Insoluble sulfates	3	2	±3%	+3	+2	▲
Salt anomalies	3	1	±3%	+3	−2	▲▲▲
Seismic hazard	1	2	±5%	+2	+1	▲
Prox. wells/areas	1	1	±8%	+1	+1	=
Urban/natural areas	2	2	±5%	+2	+1	▲
Infrastructure	3	1	±3%	+3	+1	▲▲
Brine management	2	1	±5%	+2	+1	▲
Water availability	2	1	±5%	+2	+1	▲
Location	1	2	±3%	+3	+2	▲

The comparison highlights a consistent pattern: operational sites achieve +3 robustness for the majority of parameters, with the largest discrepancy in 'salt anomalies' (+3 vs -2, a five-class gap). This parameter serves as a diagnostic indicator of operational maturity: at Realmonte, no systematic anomaly testing has been performed, whereas at Teesside and Clemens Dome, decades of continuous cycling provide the strongest possible form of validation. The tables 6-7 also demonstrate that Realmonte's data quality from its ~40 borehole mining campaign (+2 for most rock salt parameters) is already sufficient for a robust pre-feasibility assessment, and that the primary pathway to increasing robustness is operational validation through pilot cavern testing.

The CRS workflow is designed for iterative application. As new monitoring, logging, or seismic data become available during construction or operation, the site card can be updated by revising the impact and robustness values for the affected parameters. This would automatically propagate through the normalization formula (Equation 3) and the GIS-based risk maps. For example, acquisition of a 2D/3D seismic survey would improve the robustness of structural complexity and fault occurrence parameters (from robustness +1 to +2), narrowing the MC perturbation range and increasing confidence in the total score. The Monte Carlo sensitivity framework provides a built-in mechanism to quantify the information value of new data: by re-running the MC simulation before and after a data update, one can directly measure the reduction in score uncertainty (ΔCV) attributable to the new data.

5.4 Storage capacity estimate

The final CRS map for the First Cycle (Fig. 5) identifies a favourable zone (CRS > 0.5) extending over approximately 2-3 km² in the central and eastern sectors of the study area, where salt thickness exceeds 200 m, caprock integrity is high, and structural risk is low (Fig. 8). Assuming cavern heights of 100-200 m and diameters of 60-80 m, consistent with current engineering practice for salt cavern hydrogen storage, and a conservative pillar spacing of three times the cavern diameter (180-240 m centre-to-centre), the favourable area could accommodate an estimated 15-35 caverns depending on cavern dimensions (Fig. 9). For smaller caverns (100 m height, 60 m diameter, geometric volume ~0.28×10^6 m³), working gas capacity is estimated at approximately 40-60 GWh per cavern; for larger caverns (200 m height, 80 m diameter, geometric volume ~1.0×10^6 m³), working gas capacity reaches 100-150 GWh per cavern at typical operating pressures (80-100 bar). The total prospective storage capacity for the Realmonte First Cycle is therefore in the range of 1.5-2.5 TWh.

Preliminary geomechanical feasibility is supported by the depth range of the First Cycle (400-600 m below sea level), which falls within the optimal pressure envelope for salt cavern hydrogen storage (40-100 bar operating pressure at lithostatic gradients typical of bedded salt). The proposed cavern spacing of at least three times the cavern diameter (≥ 180-240 m centre-to-centre) is consistent with published pillar stability criteria for bedded salt formations [13,15]. Detailed geomechanical modelling of cavern convergence rates, operating pressure windows, and long-term creep behaviour is beyond the scope of this screening study and will require site-specific laboratory testing (e.g., triaxial creep tests on Realmonte halite cores) as part of a future feasibility assessment.
Based on the proposed cavern dimensions (100-200 m height, 60-80 m diameter), each cavern would generate approximately $0.3\text{-}0.8 \times 10^6$ m³ of saturated brine during solution mining. For 15-35 caverns, total brine production would be in the range of $5\text{-}28 \times 10^6$ m³. The coastal location of the Realmonte site enables direct marine discharge, the most cost-effective disposal option, subject to environmental impact assessment and compliance with Mediterranean marine discharge regulations.

This estimate can be considered in relation to Sicily’s projected hydrogen storage demand. Sicily is Italy’s leading region for renewable energy, with 2.6 GW of installed solar and 2.5 GW of wind capacity as of 2024, and up to 1.2 GW of offshore wind projects planned along the western and southern coasts. Current wind curtailment in Sicily reaches approximately 30% due to the lack of medium-term storage infrastructure. National projections indicate a hydrogen storage demand of approximately 6 TWh/year by 2030 and 36 TWh/year by 2050. Assuming Sicily’s proportional share at 10-15% of the national requirement, the island’s storage demand would amount to approximately 0.6-0.9 TWh by 2030 and 3.6-5.4 TWh by 2050. The estimated capacity of the Realmonte First Cycle (1.5-2.5 TWh) would therefore be sufficient to meet Sicily’s entire hydrogen storage needs through the 2030 horizon with as few as *5-8 medium-sized caverns* and could cover a substantial fraction of the 2050 demand. The site’s coastal location further enhances its strategic value, as it offers direct access to water for solution mining, brine disposal pathways, and proximity to planned offshore renewable energy generation hubs including the Med Wind floating wind farm (approximately 80 km offshore).

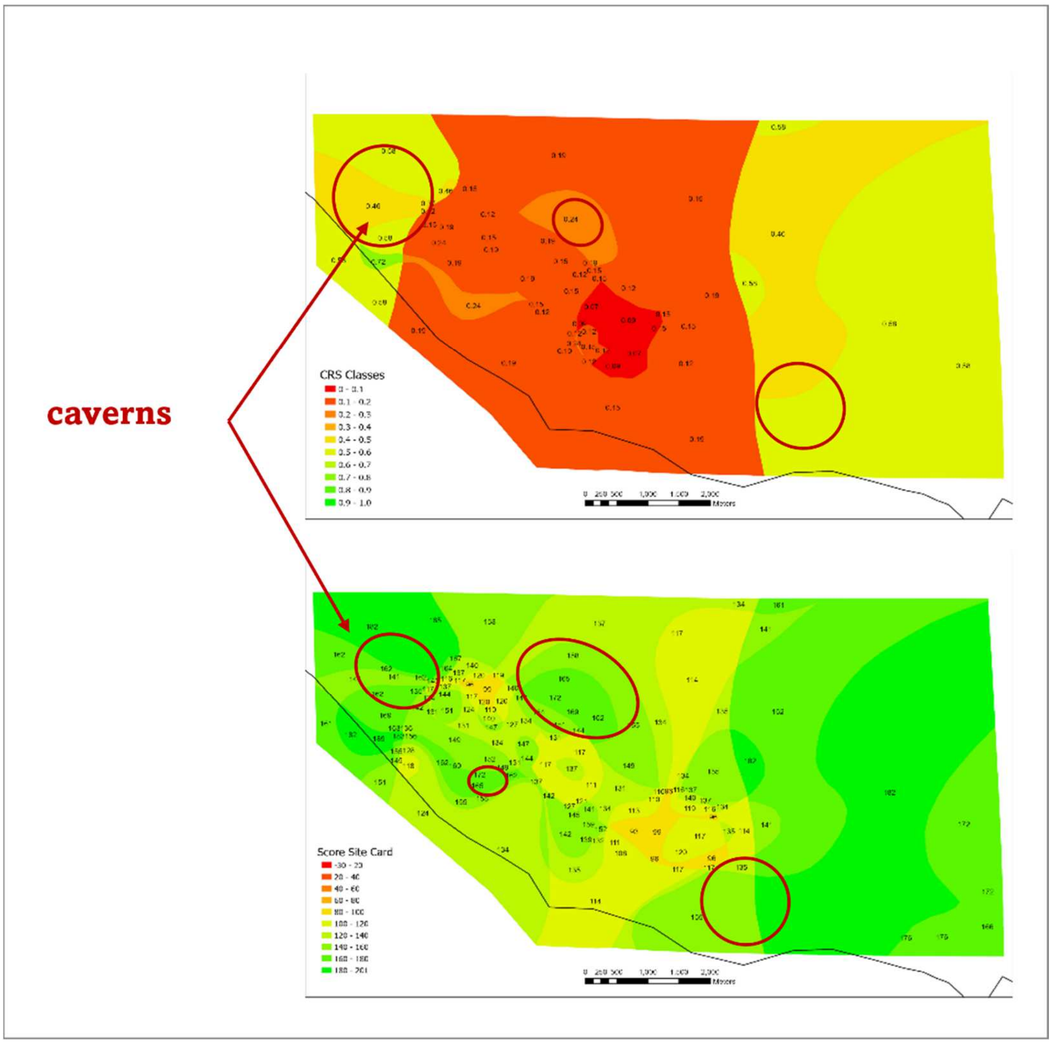

Fig.9. Integrated CRS map with cavern positions overlay

6. Conclusions

This study applied the Common Risk Segment (CRS) methodology to assess the feasibility of hydrogen storage in salt caverns at the Realmonte salt mine in southwestern Sicily, Italy. Two distinct sections of the salt deposit were evaluated: the deeper “First Cycle” and the shallower “Second Cycle”. Each was assessed using geological, structural, and environmental parameters in order to determine its suitability for hydrogen storage.

The findings of the investigation indicate that:

- he First Cycle, located below -250 m, exhibits significantly more favourable characteristics for hydrogen storage. This deeper section combines greater depth, which improves pressure containment and reduces leakage risk, with a purer halite composition, thereby minimising potential interactions between stored hydrogen and the host rock. It also shows favourable structural conditions, with limited complexity that could otherwise compromise cavern stability.

- By contrast, the Second Cycle, which include the active mine area, presents substantially greater risks and constraints for hydrogen storage. Its shallower depth raises concerns about maintaining adequate pressure containment, while its greater mineralogical heterogeneity may lead to leaching complications and potential contamination issues. The presence of mining infrastructure within the same interval introduces an additional operational conflict that further reduces its suitability. Environmental factors are generally favourable for both cycles, and the coastal location and low seismic hazard further enhance the overall attractiveness of the site.

Overall, the study demonstrates that the deeper First Cycle has significant potential for hydrogen storage and is well aligned with Sicily's expanding renewable energy sector and the growing need for large-scale energy storage solutions. This part of the salt deposit offers the most suitable conditions for the development of safe and efficient hydrogen storage facilities, which could play an important role in balancing the intermittency of wind and solar power. By identifying the most promising areas for cavern development and highlighting the main limiting factors, the study provides a robust basis for future infrastructure planning and energy policy decisions. Large-scale hydrogen storage at Realmonte could make a substantial contribution to Sicily's ambition to become a renewable energy hub and could support the island's transition toward a more resilient and sustainable energy system.

More broadly, the successful development of hydrogen storage at Realmonte could provide a model for similar projects elsewhere, demonstrating the potential for repurposing or expanding around existing salt mining districts for clean energy storage. The combination of CRS-based scoring, Monte Carlo sensitivity analysis, and cross-site benchmarking against two operational facilities (Teesside and Clemens Dome) provides a degree of methodological validation that, to the authors' knowledge, has not been achieved by previous site-screening approaches for underground hydrogen storage.
The convergence of geological suitability (CRS score 95.81%), scoring stability (CV = 0.14%), and prospective storage capacity (1.5-2.5 TWh) identifies the Realmonte First Cycle as a priority candidate for pilot cavern development in the Italian hydrogen storage roadmap.

Acknowledgments: The authors gratefully acknowledge ITALKALI for providing access to the geological and mining data of the Realmonte mine. Special thanks are due to Eng. Cristian Sabatino (Director of Realmonte Mine) and Eng. Michele Simili for their continuous support, open collaboration, and availability throughout all phases of this research. We do thanks Schlumberger for releasing an academic license of Petrel. This PhD thesis has been funded by PON Ricerca e Innovazione'' 2014-2020 Azione IV ''Dottorati su tematiche Green'' CUO E65F21003740003.

References

[1] Tarkowski R. (2019). Underground hydrogen storage: Characteristics and prospects. Renewable and Sustainable Energy Reviews, 105, 86-94. https://doi.org/10.1016/j.rser.2019.01.051

[2] Butler, R.W., Lickorish, H., Grasso, M., Pedley, H.M., & Ramberti, L. (1995). Tectonics and sequence stratigraphy in Messinian basins, Sicily: Constraints on the initiation and termination of the

Mediterranean salinity crisis. Geological Society of America Bulletin, 107, 425-439. DOI:10.1130/0016-7606(1995)107<0425:TASSIM>2.3.CO;2

[3] Caglayan, D., Weber, N., Heinrichs, H., Linssen, J., Robinius, M., Kukla, P., & Stolten, D. (2020). Technical potential of salt caverns for hydrogen storage in Europe. International Journal of Hydrogen Energy, 45, 6793-6805. https://doi.org/10.1016/j.ijhydene.2019.12.161

[4] Zhu, S., Shi, X., Yang, C., Bai, W., Wei, X., Yang, K., Li, P., Li, H., Li, Y., & Wang, G. (2024). Site selection evaluation for salt cavern hydrogen storage in China. Renewable Energy, 224, 120088. https://doi.org/10.1016/j.renene.2024.120143

[5] Huang, L., Fang, Y., Hou, Z., Xie, Y., Luo, J., Wu, L., Wang, Q., Guo, Y., & Sun, W. (2024). A preliminary site selection system for underground hydrogen storage in salt caverns and its application in Pingdingshan, China. Deep Underground Science and Engineering, 3(1), 117–128. https://doi.org/10.1002/dug2.12069

[6] Derakhshani, R., Lankof, L., GhasemiNejad, A., & Zaresefat, M. (2024). Artificial intelligence-driven assessment of salt caverns for underground hydrogen storage in Poland. Scientific Reports, 14, 14246. https://doi.org/10.1038/s41598-024-64020-9

[7] Lankof, L., Urbańczyk, K., & Tarkowski, R. (2022). Assessment of the potential for underground hydrogen storage in salt domes. Renewable and Sustainable Energy Reviews, 160, 112309. https://doi.org/10.1016/j.rser.2022.112309

[8] Baek, S., Ruiz Maraggi, L.M., & Moscardelli, L.G. (2024). SHASTA: Salt cavern hydrogen storage assessment tool. U.S. Department of Energy.

[9] Grant, S.M., Milton, N.J., & Thompson, M. (1996). Play fairway analysis and risk mapping: an example using the Middle Jurassic Brent Group in the northern North Sea. In: Doré, A.G. & Sinding-Larsen, R. (Eds.), Quantification and Prediction of Petroleum Resources. Norwegian Petroleum Society Special Publications, 6, 167-181. https://doi.org/10.1016/S0928-8937(07)80017-8

[10] Bump, A.P., Hovorka, S.D., & Meckel, T.A. (2021). Common risk segment mapping: Streamlining exploration for carbon storage sites, with application to coastal Texas and Louisiana. International Journal of Greenhouse Gas Control, 111, 103457. https://doi.org/10.1016/j.ijggc.2021.103457

[11] Barnett, H.G., Ireland, M.T., & Van Der Land, C. (2025). Capturing geological uncertainty in salt cavern developments for hydrogen storage. Earth Science, Systems and Society. https://doi.org/10.3389/esss.2024.10125

[12] Williams, J.D.O., Williamson, J.P., Parkes, D., Evans, D.J., Kirk, K.L., Sunny, N., Hough, E., Vosper, H., & Akhurst, M.C. (2022). Does the United Kingdom have sufficient geological storage capacity to support a hydrogen economy? Estimating the salt cavern storage potential of bedded halite formations. Journal of Energy Storage, 53, 105109. https://doi.org/10.1016/j.est.2022.105109

[13] Evans, D.J. (2008). An appraisal of underground gas storage technologies and incidents, for the development of risk assessment methodology. HSE Research Report RR605, 287 pp.

[14] Stone, H.B.J., Veldhuis, I., & Richardson, R.N. (2009). Underground hydrogen storage in the UK. In: Evans, D.J. & Chadwick, R.A. (Eds.), Underground Gas Storage: Worldwide Experiences and Future Development in the UK and Europe. Geological Society, London, Special Publications, 313, 217–226. https://doi.org/10.1144/SP313.13

[15] Crotogino, F., Schneider, G.-S., & Evans, D.J. (2018). Renewable energy storage in geological formations. Proceedings of the Institution of Mechanical Engineers, Part A: Journal of Power and Energy, 232(1), 100–114. https://doi.org/10.1177/0957650917731181

[16] Ruiz Maraggi, L.M., & Moscardelli, L. (2023). Modeling hydrogen storage capacities, injection and withdrawal cycles in salt caverns: Introducing the GeoH2 salt storage and cycling app. International Journal of Hydrogen Energy, 48(71), 26921–26936. https://doi.org/10.1016/j.ijhydene.2023.03.293

[17] Nobian. Storage caverns. https://www.nobian.com/our-activities/storage-caverns

[18] Regione Siciliana. Strategia regionale idrogeno. Dipartimento Energia, Assessorato Energia e Servizi di Pubblica Utilità. https://www.regione.sicilia.it/istituzioni/regione/strutture-regionali/assessorato-energia-servizi-pubblica-utilita/dipartimento-energia/strategia-regionale-idrogeno

[19] Ministero della Transizione Ecologica. Progetto di un parco eolico offshore denominato "Eureka Wind", costituito da 38 aerogeneratori della potenza complessiva di 570 MW. https://va.mite.gov.it/it-IT/Oggetti/Info/11207

[20] Ministero della Transizione Ecologica. Progetto di un parco eolico offshore flottante denominato "Bluwind Pozzallo" con potenza complessiva pari a 975 MW. https://va.mite.gov.it/it-IT/Oggetti/Info/9882

[21] Ministero della Transizione Ecologica. Progetto per parco eolico offshore denominato "Ostro" composto da 40 turbine eoliche galleggianti, per una potenza complessiva di circa 600 MW. https://va.mite.gov.it/it-IT/Oggetti/Info/8665

[22] Ministero della Transizione Ecologica. Progetto di un impianto eolico offshore di tipo floating composto da 21 aerogeneratori per una potenza complessiva pari a 250 MW ("7Seas Med"). https://va.mite.gov.it/it-IT/Oggetti/Info/8378

[23] Ministero della Transizione Ecologica. Progetto per la realizzazione di un parco eolico offshore di tipo galleggiante denominato "Sicilia A" della potenza di 1020 MW. https://va.mite.gov.it/it-IT/Oggetti/Info/9399

[24] Ministero della Transizione Ecologica. Progetto per la realizzazione di un parco eolico offshore di tipo floating denominato "Sicily South" per una potenza nominale complessiva di 1200 MW. https://va.mite.gov.it/it-IT/Oggetti/Info/9331

[25] Ministero della Transizione Ecologica. Progetto di un impianto eolico offshore di tipo floating denominato "Calypso", composto da 40 aerogeneratori da 15 MW ciascuno, per una potenza complessiva pari a 600 MW. https://va.mite.gov.it/it-IT/Oggetti/Documentazione/8570

[26] Agenzia Europea dell'Ambiente. EUNIS - European Nature Information System: ITA040015. https://eunis.eea.europa.eu/sites/ITA040015

[27] Axpo. (2024, April 9). Axpo H2 Sicily [PDF]. https://www.axpo.com/content/dam/axpo19/master/files-master/media-releases/2024/240409_Axpo_H2_Sicily_EN.pdf

[28] Lugli, S., Manzi, V., Roveri, M., & Schreiber, B. (2010). The Primary Lower Gypsum in the Mediterranean: A new facies interpretation for the first stage of the Messinian Salinity Crisis.

Palaeogeography, Palaeoclimatology, Palaeoecology, 297, 83-99. https://doi.org/10.1016/j.palaeo.2010.07.017

[29] Roveri, M., Manzi, V., Lugli, S., Schreiber, B., Caruso, A., Rouchy, J.-M., Iaccarino, S., Gennari, R., Vitale, F., & Lucchi, F. (2006). Clastic vs. primary precipitated evaporites in the Messinian Sicilian basins. L'Ateneo Parmense. Acta Naturalia, 42, 125-199.

[30] Lugli, S. (1999). Geology of the Realmonte salt deposit, a desiccated Messinian Basin (Agrigento, Sicily). Società Geologica Italiana Memorie, 54, 75-81.

[31] Decima, A., & Wezel, F.C. (1971). Osservazioni sulle evaporiti messiniane della Sicilia centro-meridionale. Rivista Mineralogica Siciliana, 22, 130-132.

[32] Roveri, M., & Lugli, S., Manzi, V., & Schreiber, B. (2008). The Messinian salinity crisis: A sequence-stratigraphic approach. Geoacta Special Publication, 117-138.

[33] Samperi, L., Giorgio, M., Kamaldeen, O.O., Zappone, A., Waldmann, N., Nazzareni, S., Pauselli, C., & Bianchi, F. (2020). Estimation of the physical, petrophysical and mineralogical properties of Messinian salt rocks, Sicily: Implications for multidisciplinary applications. Marine and Petroleum Geology, 112, 104032. https://doi.org/10.1016/j.marpetgeo.2019.104032

[34] Anzelmo, G., Cella, G.M., Magistroni, C., Da Pra, A., & Iacopini, D. (submitted). Methodological workflow for screening and ranking of salt caverns for underground hydrogen storage: the CRS approach.

[35] Decima, A. (1978). Initial data on bromine distribution in the Miocene salt formation of southern Sicily. Memorie della Società Geologica Italiana, 16, 39-43.